Volume 4 | Number 34 | 14 September 2016 | Pages 5631–5762

Journal of Materials Chemistry B

Materials for biology and medicine

www.rsc.org/MaterialsB

ISSN 2050-750X

ROYAL SOCIETY OF CHEMISTRY

COMMUNICATION

Yuming Guo, Lin Yang *et al.*

Facile green synthesis of calcium carbonate/folate porous hollow spheres for the targeted pH-responsive release of anticancer drugs

175 YEARS

Journal of Materials Chemistry B

COMMUNICATION

View Article Online
View Journal | View Issue

Cite this: J. Mater. Chem. B, 2016, 4, 5650

Received 16th June 2016,
Accepted 24th July 2016

DOI: 10.1039/c6tb01483f

www.rsc.org/MaterialsB

Facile green synthesis of calcium carbonate/folate porous hollow spheres for the targeted pH-responsive release of anticancer drugs†

Yuming Guo,*[ab] Weili Jia,[a] Han Li,[a] Weike Shi,[a] Jie Zhang,[a] Jing Feng[a] and Lin Yang*[ab]

Biocompatible hybrid hollow spheres of calcium carbonate/folate with both mesopores and macropores were synthesized using a facile green approach based on Ostwald ripening. The porous hollow spheres were efficiently loaded with doxorubicin, which they were then able to release in a pH-responsive and sustained manner for the targeted treatment of human cancer cells.

The efficacy of chemotherapeutic drugs is often unsatisfactory as a result of poor tumour specificity and serious side-effects.[1] Drug delivery systems (DDSs) have therefore attracted much attention because they can augment the efficacy of treatment and significantly reduce side-effects.[2] Facile synthesis, long-term stability, biocompatibility, a high loading efficiency and targeted delivery to cancer cells are all important factors in the practical application of DDSs.[3] It is crucial that the release of the drug is triggered in a sustained manner by stimuli associated with specific microenvironmental changes.[4] Most of the DDSs reported to date have been based on polymers.[5] However, their complex synthesis, the use of toxic agents, complex degradation products and potential side-effects have greatly limited their application. Inorganic materials such as mesoporous silica are promising candidates for DDSs because they have a number of advantages over synthetic polymers, including simple preparation and the reduced use of toxic agents.[6] Compared with silica, $CaCO_3$ has good biocompatibility and biodegradability and may be an ideal candidate for use in DDSs.[7,8]

Bimodal porous $CaCO_3$/folate (FA) hybrid hollow spheres ($CaCO_3$/FA HSs) were prepared under ambient conditions using a facile green method without any toxic agents. Time-dependent SEM observations suggested that the formation mechanism of the HSs was Ostwald ripening. Because of the special morphological features of the product (the presence of a hollow cavity and bimodal pores), we were able to load the $CaCO_3$/FA HSs with the anticancer drug doxorubicin (DOX). As a result of the pH sensitivity, good biocompatibility and biodegradability of $CaCO_3$, the $CaCO_3$/FA HSs we able to release DOX in a controlled and sustained manner after triggering by the weak acidic microenvironment of cancer cells. The FA molecules on the $CaCO_3$/FA HSs bound specifically to the folate receptor (FR) that is overexpressed on cancer cells. The specificity of DOX between normal cells and cancer cells was enhanced 5.19-fold by loading onto the $CaCO_3$/FA HSs. These results suggest that $CaCO_3$/FA HSs could be used as a DDS to specifically treat human cancers. Combined with our previous reports,[7,9] this study further illustrates the potential of inorganic materials to act as drug carriers for the efficient treatment of human cancers.

Scheme 1 shows the facile preparation of $CaCO_3$/FA HSs, the efficient loading of DOX, the targeted delivery and the specific and significant inhibition of cancer cell proliferation. Aqueous solutions of FA (2.5 mM, 12.5 mL) and $CaCl_2$ (5 mM, 12.5 mL) were mixed at 25 °C in a molar ratio of 1 : 2. An aqueous solution of Na_2CO_3 (2.5 mM, 25 mL) was then added and incubated for 24 h at 25 °C to prepare the HSs. DOX was loaded into the HSs and was delivered to the cancer cells based on the highly specific interaction of FA with the FR overexpressed on the membrane of the cancer cells. The $CaCO_3$/FA/DOX spheres were specifically internalized by the cancer cells through macropinocytosis. The $CaCO_3$ decomposed in the cells, releasing the DOX.

The size and morphology of the $CaCO_3$/FA HSs were determined by SEM and TEM. The $CaCO_3$/FA HSs were well-dispersed hollow spheres with an average diameter of 1.52 ± 0.01 μm and a shell thickness of 300 nm (Fig. 1a and Fig. S1a, ESI†). FESEM analysis demonstrated that the $CaCO_3$/FA HSs were composed of nanoclusters with an average size of 22.23 ± 0.41 nm (Fig. 1b and Fig. S1b, ESI†). The control product prepared in the absence of FA did not consist of hollow spheres, but were cubic-like aggregates (Fig. S1c, ESI†). This shows that FA plays an important part in the preparation of the $CaCO_3$/FA HSs.

[a] Collaborative Innovation Center of Henan Province for Green Manufacturing of Fine Chemicals, Key Laboratory of Green Chemical Media and Reactions, Ministry of Education, Henan Normal University, Xinxiang, Henan 453007, P. R. China. E-mail: guoyuming@htu.edu.cn, yanglin1819@163.com

[b] Henan Key Laboratory of Green Chemical Media and Reactions, School of Chemistry and Chemical Engineering, Henan Normal University, Xinxiang, Henan 453007, P. R. China

† Electronic supplementary information (ESI) available: Experimental details and supplementary results. See DOI: 10.1039/c6tb01483f

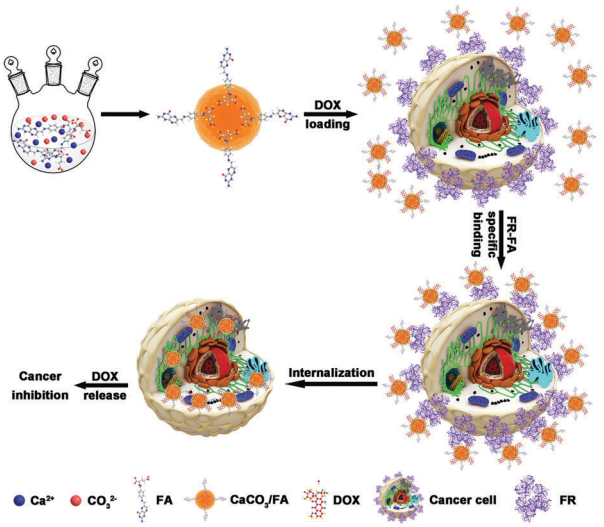

Scheme 1 Preparation of $CaCO_3$/FA HSs, efficient loading of DOX, targeted delivery, specific internalization and inhibition of cancer cells.

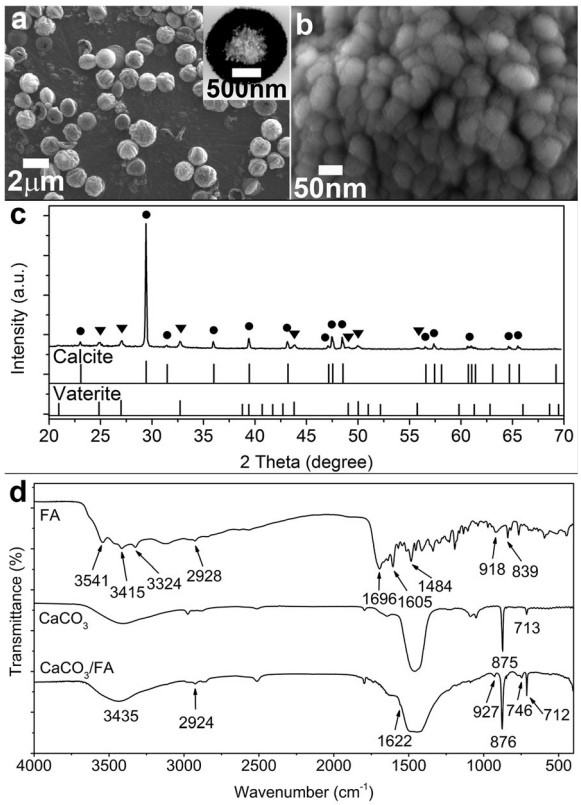

Fig. 1 (a) SEM and (b) FESEM images of $CaCO_3$/FA HSs. Inset: TEM image. (c) XRD patterns of FA, $CaCO_3$ and $CaCO_3$/FA HSs. The diffraction peaks of calcite and vaterite are highlighted by closed circles and closed triangles, respectively. (d) FTIR spectra of FA, $CaCO_3$ and $CaCO_3$/FA HSs.

Fig. 1c shows the XRD pattern obtained for the $CaCO_3$/FA HSs. The diffraction peaks highlighted by the closed circles and closed triangles were assigned to calcite and vaterite, respectively, indicating the simultaneous presence of these two phases. The FTIR spectra in Fig. 1d show that, in addition to the characteristic peaks of calcite[10] at 712 and 876 cm^{-1} and vaterite at 746 cm^{-1} in the spectrum of $CaCO_3$/FA HSs,[11] the absorption peaks at 3435, 1622 and 927 cm^{-1} could be assigned to the (N–H), (C═O) and (O–H) bonds of FA, respectively.[12] This clearly indicates that the $CaCO_3$/FA HSs are composed of calcite, vaterite and FA. The obvious shift in the absorption peaks indicated the static electronic interactions between FA and $CaCO_3$. The control $CaCO_3$ showed only the characteristic peaks of calcite. TG-DSC analysis (Fig. S1d, ESI†) showed a mass loss from 100 to 610 °C of 2.09%, which can be attributed to the combustion of FA.

To investigate the process of formation of the $CaCO_3$/FA HSs, the intermediate products present after different reaction times were monitored (Fig. 2 and Fig. S2, ESI†). Fig. 2a shows that $CaCO_3$/FA nanoparticles were obtained after reaction for 10 min. When the reaction time was increased to 3 h, solid spheres with an average diameter of 0.79 μm were produced (Fig. 2b). When the reaction time reached 6 h, the diameter of the solid spheres increased to 1.17 μm (Fig. 2c). After 12 h, 1.31 μm spheres with inner cavities were produced (Fig. 2d). With further increases in the reaction time to 18 and 24 h, hollow spheres with average diameters of 1.48 and 1.52 μm were obtained (Fig. 2e and f). Based on these results, the formation mechanism of the HSs can be explained as Ostwald ripening (Scheme 2).[13] In the early stages, tiny $CaCO_3$/FA nanoparticles were quickly produced through the reaction of Ca^{2+} with CO_3^{2-} and these nanoparticles spontaneously aggregated to form large solid spheres to minimize their surface energy. The particles in the inner core can be considered as smaller spheres with a higher curvature than those on the outer surface. During the later stages, these particles dissolved and merged into the particles on the outer surface as a result of the higher surface energy, forming structures with a hollow interior.

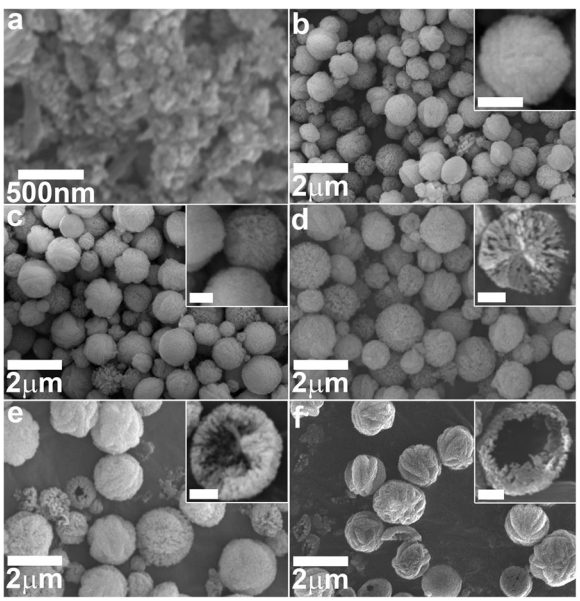

Fig. 2 SEM images showing the evolution of $CaCO_3$/FA HSs after different reaction times: (a) 0.5; (b) 3; (c) 6; (d) 12; (e) 18; and (f) 24 h. Insets: Magnified SEM images; scale bars 500 nm.

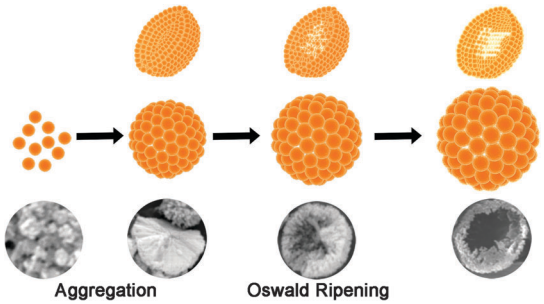

Scheme 2 Formation mechanism of $CaCO_3$/FA HSs. Top: Model cross-section of samples at different steps. Bottom: SEM images of samples at different steps.

The effects of the preparation conditions on the morphology of the products were determined. The results indicated the importance of the molar ratios of FA/Ca^{2+} and pH. It was seen from the SEM observations that the products for the 1 : 1, 1 : 3, 1 : 5 and 2 : 1 molar ratios were not hollow spheres, but tetrapod-like aggregates (1 : 1 and 1 : 3), irregular aggregates (1 : 5) and cubic aggregates (2 : 1), respectively (Fig. S3a–d, ESI†). When the pH of the reaction system was increased, the products were no longer hollow spheres, but had an irregular morphology at pH 9 and were cubes at pH 11 (Fig. S3e and f, ESI†).

The specific surface area of the $CaCO_3$/FA HSs was determined to be 22.68 $m^2\ g^{-1}$ by multipoint BET analysis (Fig. 3a). Analysis of the pore size distribution indicated a bimodal porosity. Fig. 3b shows two sets of pores with diameters centred at 11.8 and 63.2 nm, indicating the simultaneous presence of mesopores and macropores.[14] FESEM observations confirmed this result (Fig. 3c and d). The pores of $CaCO_3$/FA HSs provide spaces into which drugs can be loaded.

Using DOX as a model drug, the potential application of $CaCO_3$/FA HSs as a carrier for anticancer drugs was studied. The red autofluorescence of DOX was used to monitor the loading effect. The strong red autofluorescence of $CaCO_3$/FA/DOX indicated the efficient loading of DOX (Fig. 3e); loading and entrapment were determined to be 8.637 and 86.37%, respectively. This could be attributed to the presence of the bimodal pores in the $CaCO_3$/FA HSs.

The evaluation of the *in vitro* release of DOX showed that the $CaCO_3$/FA HSs could be used as a DDS for the pH-responsive and sustained release of DOX. In general, the microenvironment of tumour tissues is more acidic than that of normal tissues.[15] This intrinsic feature of tumour phenotypes can be used as a stimulus for drug release in pH-sensitive DDSs. Therefore the *in vitro* release of $CaCO_3$/FA/DOX was evaluated at different pH values to simulate tumours and normal tissues. Fig. 3f shows that the release performance under acidic conditions was much better than under normal physiological conditions. This can be ascribed to the gradual decomposition of $CaCO_3$ under acidic conditions, which was confirmed by the observed morphological changes. $CaCO_3$/FA HSs incubated in a neutral release buffer remained as spheres (Fig. 3g). However, $CaCO_3$/FA HSs incubated in acidic buffers broke into small pieces (Fig. 3h and i), demonstrating the gradual decomposition of $CaCO_3$ under acidic conditions. These results suggest that the $CaCO_3$/FA HSs could be used as a

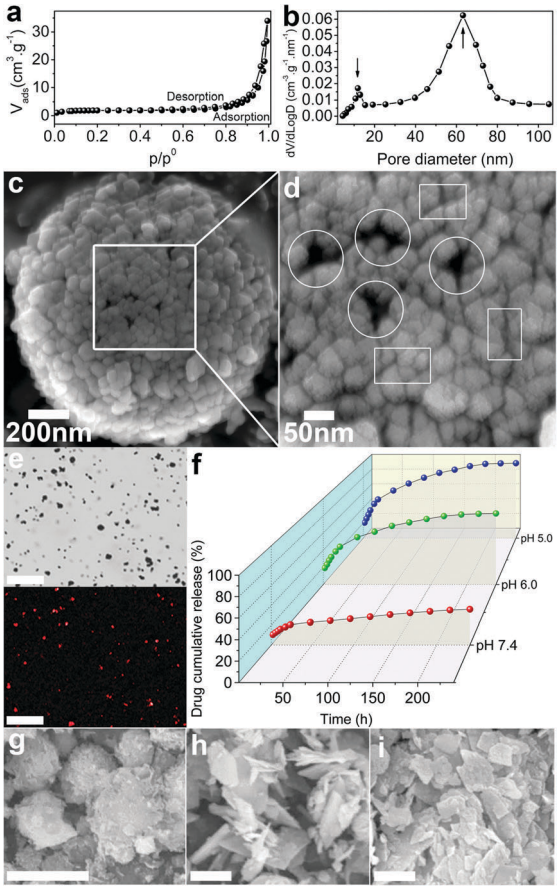

Fig. 3 (a) Nitrogen adsorption/desorption isotherm, (b) pore size distribution and (c and d) FE-SEM images of $CaCO_3$/FA HSs. The circles and rectangles in (d) highlight the macropores and mesopores, respectively. (e) Light (upper panel) and fluorescence (lower panel) micrographs of $CaCO_3$/FA/DOX. Scale bar 50 μm. (f) *In vitro* release profiles of $CaCO_3$/FA/DOX at different pH values. Each data point represents the mean ± SD value; n = 6. (g–i) SEM images of $CaCO_3$/FA HSs incubated for 3 d in release buffers of pH 7.4, 6.0 and 5.0, respectively. Scale bars 2 μm.

pH-sensitive carrier to release anticancer drugs in response to the acidic microenvironment of tumours. The release of DOX occurred in a sustained manner over a 10-day period. This allowed the DOX to exert anticancer activity at the correct level for much longer than the pure component, which is beneficial in reducing the frequency of administration.

The cytotoxic effects of DOX and $CaCO_3$/FA/DOX on V79-4 normal cells and HeLa cancer cells were determined to evaluate the delivery and release efficiency of $CaCO_3$/FA/DOX. Fig. 4a and b shows that after 3 days of treatment the IC_{50} of $CaCO_3$/FA/DOX for V79-4 cells was 0.2393 μg mL^{-1}, much higher than that of free DOX (0.1359 μg mL^{-1}). This indicates the reduction in the undesirable side-effects of DOX by loading onto the $CaCO_3$/FA HSs. The IC_{50} of $CaCO_3$/FA/DOX for HeLa cells was 0.0271 μg mL^{-1}, significantly lower than that of free DOX (0.0798 μg mL^{-1}). This revealed an augmentation of the desirable anticancer effects of DOX after loading onto the $CaCO_3$/FA HSs. The light micrographs of the V79-4 and HeLa cells before and after treatment with $CaCO_3$/FA/DOX further confirmed the specific inhibitory effects of $CaCO_3$/FA/DOX on cancer cells (Fig. S4a–d, ESI†).

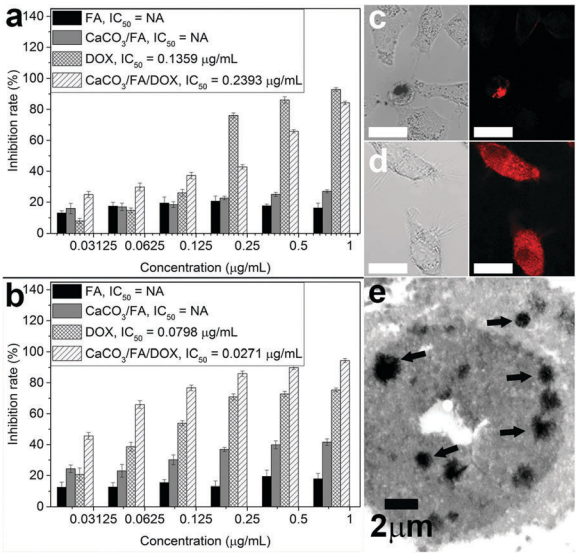

Fig. 4 Cytotoxic effects of FA, free DOX, $CaCO_3$/FA and $CaCO_3$/FA/DOX on (a) V79-4 and (b) HeLa cells after 3 d of treatment (n = 6). Light (left) and fluorescence (right) micrographs of (c) V79-4 cells and (d) HeLa cells after treatment with $CaCO_3$/FA/DOX for 12 h. Scale bar 20 μm. (e) TEM image of HeLa cells after treatment with $CaCO_3$/FA/DOX for 12 h. The dark arrows highlight the $CaCO_3$/FA/DOX within the HeLa cell.

As a cysteine-rich membrane glycoprotein, FR is often over-expressed in cancer cells and can specifically combine with FA through ligand–receptor interactions.[16] Fig. 4c and d shows that the HeLa cells rather than the normal cells emitted a strong red autofluorescence of DOX after treatment with $CaCO_3$/FA/DOX, which might be attributed to the targeted delivery and macropinocytosis of the $CaCO_3$/FA/DOX into HeLa cells. The TEM image of the HeLa cell after treatment with $CaCO_3$/FA/DOX (Fig. 4e) clearly shows the presence of $CaCO_3$/FA/DOX within the HeLa cells. This further supports the macropinocytosis of $CaCO_3$/FA/DOX by the HeLa cells.

For a chemotherapeutic drug, the specificity between the normal and cancer cells can be defined as the ratio of the IC_{50} value for normal cells to that for cancer cells. A higher IC_{50} ratio represents better specificity.[17] Based on this concept, the specificities of free DOX and $CaCO_3$/FA/DOX were calculated as 1.70 and 8.83, respectively. The specificity of DOX was significantly increased 5.19-fold by loading onto the $CaCO_3$/FA HSs. This can be attributed to the targeted delivery of $CaCO_3$/FA/DOX to cancer cells.

ICP-MS showed that the $[Ca^{2+}]$ in $CaCO_3$/FA/DOX treated HeLa cells was 153.2 mg L^{-1}, much higher than the concentration in the culture medium (82.7 mg L^{-1}) and V79-4 cells (105.3 mg L^{-1}). This might be attributed to the gradual dissolution and decomposition of $CaCO_3$ in the weak acidic microenvironment of HeLa cells, which resulted in the sustained release of DOX.

Porous $CaCO_3$/FA HSs were successfully prepared through a facile green strategy. The characteristics of $CaCO_3$/FA HSs, including the presence of bimodal pores, the specific ligand–receptor interaction between FA and FR, and the pH sensitivity, resulted in the effective loading, targeted delivery, pH-responsiveness and sustained release of anticancer drugs to specifically treat human cancers. These results suggest that inorganic microscale materials might be used as DDSs to specifically treat human cancers.

This work was financially supported by the National Natural Science Foundation of China (21271066, U1204516, 21571053) and the Program for Science & Technology Innovation Talents in Universities of Henan Province (13HASTIT011).

Notes and references

1 (*a*) E. Jin, B. Zhang, X. Sun, Z. Zhou, X. Ma, Q. Sun, J. Tang, Y. Shen, E. Van Kirk and W. J. Murdoch, *J. Am. Chem. Soc.*, 2013, **135**, 933; (*b*) E. A. Kuczynski, D. J. Sargent, A. Grothey and R. S. Kerbel, *Nat. Rev. Clin. Oncol.*, 2013, **10**, 571.
2 (*a*) B. Delalat, V. C. Sheppard, S. Rasi Ghaemi, S. Rao, C. A. Prestidge, G. McPhee, M.-L. Rogers, J. F. Donoghue, V. Pillay, T. G. Johns, N. Kroger and N. H. Voelcker, *Nat. Commun.*, 2015, **6**, 8791; (*b*) S. Mura, J. Nicolas and P. Couvreur, *Nat. Mater.*, 2013, **12**, 991.
3 P. Pamies and A. Stoddart, *Nat. Mater.*, 2013, **12**, 957.
4 (*a*) E. Kim, D. Kim, H. Jung, J. Lee, S. Paul, N. Selvapalam, Y. Yang, N. Lim, C. G. Park and K. Kim, *Angew. Chem., Int. Ed.*, 2010, **49**, 4405; (*b*) R. Mo, T. Jiang, R. DiSanto, W. Tai and Z. Gu, *Nat. Commun.*, 2014, **5**, 3364.
5 J. Nicolas, S. Mura, D. Brambilla, N. Mackiewicz and P. Couvreur, *Chem. Soc. Rev.*, 2013, **42**, 1147.
6 (*a*) F. Muhammad, M. Guo, W. Qi, F. Sun, A. Wang, Y. Guo and G. Zhu, *J. Am. Chem. Soc.*, 2011, **133**, 8778; (*b*) C.-H. Tsai, J. L. Vivero-Escoto, I. I. Slowing, I. J. Fang, B. G. Trewyn and V. S. Y. Lin, *Biomaterials*, 2011, **32**, 6234.
7 (*a*) Y. Guo, J. Zhang, L. Jiang, X. Shi, L. Yang, Q. Fang, H. Fang, K. Wang and K. Jiang, *Chem. Commun.*, 2012, **48**, 10636; (*b*) X. Ma, X. Zhang, L. Yang, G. Wang, K. Jiang, G. Wu, W. Cui and Z. Wei, *Nanoscale*, 2016, **8**, 8687.
8 G. Helmlinger, F. Yuan, M. Dellian and R. K. Jain, *Nat. Med.*, 1997, **3**, 177.
9 X. Ma, H. Chen, L. Yang, K. Wang, Y. Guo and L. Yuan, *Angew. Chem., Int. Ed.*, 2011, **50**, 7414.
10 G. Falini, S. Albeck, S. Weiner and L. Addadi, *Science*, 1996, **271**, 67.
11 C. Qi, Y.-J. Zhu, B.-Q. Lu, X.-Y. Zhao, J. Zhao, F. Chen and J. Wu, *Small*, 2014, **10**, 2047.
12 (*a*) D. Chandrasekar, R. Sistla, F. J. Ahmad, R. K. Khar and P. V. Diwan, *Biomaterials*, 2007, **28**, 504; (*b*) J. Zhang, S. Rana, R. S. Srivastava and R. D. K. Misra, *Acta Biomater.*, 2008, **4**, 40.
13 B. Liu and H. C. Zeng, *Small*, 2005, **1**, 566.
14 K. S. W. Sing, D. H. Everett, R. A. W. Haul, L. Moscow, R. A. Pieroffl, J. Rouquerol and T. Siemieni-Ewska, *Pure Appl. Chem.*, 1985, **57**, 603.
15 P. Swietach, R. D. Vaughan-Jones, A. L. Harris and A. Hulikova, *Philos. Trans. R. Soc., B*, 2014, **369**, 20130099.
16 C. Chen, J. Ke, X. E. Zhou, W. Yi, J. S. Brunzelle, J. Li, E.-L. Yong, H. E. Xu and K. Melcher, *Nature*, 2013, **500**, 486.
17 P. Phatak, F. Dai, M. Butler, M. P. Nandakumar, P. L. Gutierrez, M. J. Edelman, H. Hendriks and A. M. Burger, *Clin. Cancer Res.*, 2008, **14**, 4593.